

Generation and characterization of palladium nanocatalyst anchored on a novel polyazomethine support: Application in highly efficient and quick catalytic reduction of environmental contaminant nitroarenes

Nuray Yilmaz Baran

Aksaray University, Technical Vocational School, Department of Chemistry Technology, Aksaray, 68100, Turkey

ARTICLE INFO

Article history:

Received 28 February 2020

Received in revised form

5 June 2020

Accepted 11 June 2020

Available online 17 June 2020

Keywords:

Polyazomethines

Schiff base polymers

Palladium nanoparticles

Nitroarene reduction

ABSTRACT

Removal of toxic nitroarenes, which threaten all living organisms and environment, from wastewaters has been an important and prior issue. Therefore, the focus of the present study was to fabricate an effective, fast, reusable, and easily recoverable heterogeneous Pd nanoparticles (Pd NPs) supported on a novel polyazomethine having phenol group (Pd NPs@P(3-M-4-PAP)) for removal of several hazardous nitroarenes by catalytic reduction from water. Firstly, a novel polyazomethine featuring phenol group was prepared as a stabilizer and then, Pd NPs were anchored on it. Characterizations of the materials were performed by XRD, UV-Vis, FTIR, ¹H-NMR, TGA, FE-SEM, EDS and TEM techniques. The obtained TEM analysis results showed that the size of Pd NPs was about 50 nm. Then, catalytic ability of Pd NPs@P(3-M-4-PAP) was investigated in reduction of harmful nitroarenes to useful aniline derivatives in water. Catalytic tests revealed that Pd NPs@P(3-M-4-PAP) had outstanding catalytic efficiency against reduction of different nitroarenes by giving excellent yields (up to 98%), in very short time (between 22s and 70s) with 2 mg nanocatalyst. Moreover, performed reusability test results demonstrated that the Pd NPs@P(3-M-4-PAP) could be recurrently reusable and easily recoverable.

© 2020 Elsevier B.V. All rights reserved.

1. Introduction

Nitroarenes are known to be among the most hazardous pollutants which released to environment from the manufacturing plants of dyes, pharmaceuticals, agrochemicals, and explosives [1,2]. To exposure to even very low amount of these harmful chemicals in water can cause several problems in living organisms because of their mutagenic, carcinogenic and highly toxic effects [3]. They can lead to damages in the kidney, liver, blood, skin and central nervous systems of humans and animals [2,4]. Thus, several nitroarenes such as 4-nitrophenol (4-NP) and 2-nitroaniline (2-NA) have been included in the priority toxic pollutants list prepared by The United States Environmental Protection Agency [5]. Therefore, degradation of these hazardous pollutants to harmless products and their removal from the environment have become a vital issue for all living things. However, high stability and low solubility of these chemicals make difficult their removal process from

wastewaters. Several techniques have been proposed for their removal such as electro-Fenton method [6], photo catalysis [7], biological degradation [8], electrochemical degradation [9], thermal decomposition [10], and catalytic reduction. Catalytic reduction has recently drawn great attention of researchers compared to other methods due to its high efficiency, rapidity and economic, simple, safety and green operation [11]. Toxic nitroarenes are converted into harmless and useful aniline derivatives by catalytic reduction. Aniline derivatives which have been produced by reduction of nitroarenes are also used as intermediates in the production of several agrochemicals, antipyretic and analgesic drugs, photographic materials, dyes, pigments and polymers [12,13]. Researchers have achieved many advantages with use of heterogeneous catalysts prepared with metal nanoparticles (MNPs) in catalytic reductions of nitroarenes to aniline derivatives. In this way, while heterogeneity of the system has provided superior advantages such as easily removal of catalyst from reaction media, reusability, easily recoverability, high efficiency, and minimum palladium leaching, use of MNPs as catalyst has also gained excellent benefits such as high stability, strong electron transfer

E-mail address: nybaran@aksaray.edu.tr.

capability, large surface area, and a large number of active sites [14,15]. Although use of MNPs in catalytic systems has recently attracted tremendous interest of researchers, agglomeration and size control of nanoparticles drawbacks encountered in fabrication of MNPs have pushed researchers to be in search of new solutions [12]. Selection of suitable support material for the immobilization of MNPs has been stated as one of the best ways to overcome these problems [16]. Support material affects many catalyst properties such as activity, recoverability, reusability, and ease of removal of the catalyst from the reaction media. Moreover, suitable support material decreases the agglomeration of NPs [17,18]. Thus, it is highly desirable to generate an efficient support material for the immobilization of MNPs.

Polyazomethines which are prepared by oxidative polycondensation reactions of Schiff base monomers may be effective and ideal support materials for reduction of nitroarenes. Their high thermal and mechanical stability, outstanding optic, electrochemical, semiconductive, efficient catalyst and antibacterial, anticancer, and antitumor properties make them highly attractive as support material [19–23].

The purpose of the present research was to reveal that - a novel polyazomethine could be an efficient and suitable support material for immobilization of MNPs and - to fabricate Pd NPs as an effective and reusable heterogeneous catalyst for easy removal of toxic nitroarenes from wastewaters. Catalytic tests showed that the designed Pd NPs were a highly effective, fast, recurrently reusable, and easily recoverable nanocatalyst for removal of hazardous nitroarenes from wastewaters.

2. Experimental

2.1. Materials

3-pyridinecarboxaldehyde, 4-amino-3-methylphenol, PdCl₂, NaBH₄, 3-nitrophenol, 4-nitrophenol, 2-nitroaniline, 4-nitroaniline, 4-nitro-*o*-phenylenediamine, 4-nitrobenzoic acid, 3-nitro benzaldehyde and 4-nitro benzaldehyde, ethyl acetate, methanol, ethanol, DMF, and DMSO were obtained from Sigma-Aldrich. NaOCl (15% aqu.) was also purchased from PI-dess Chem. Co.

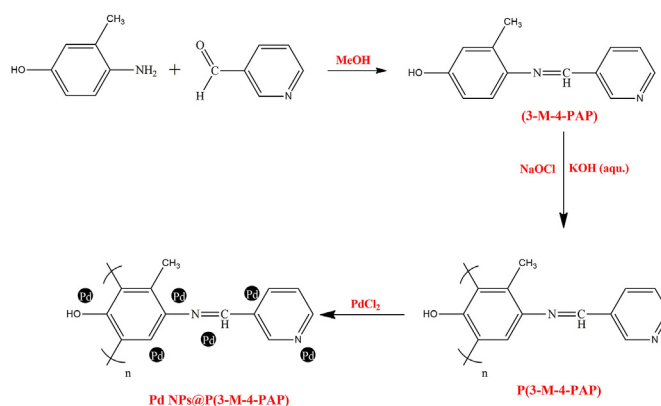
2.2. Method

2.2.1. Synthesis of 3-M-4-PAP

3-M-4-PAP was prepared by stirring 3-pyridinecarboxaldehyde (0.96 mL, 10 mmol) and 4-amino-3-methylphenol (1.23 g, 10 mmol) in methanol (25 mL) at 60 °C for 24 h using Dean–Stark apparatus. Additionally, the completion of Schiff base reaction was followed by FT-IR and TLC techniques. After the reaction, 3-M-4-PAP was filtered, washed with methanol and it was crystallized from ethyl acetate twice.

2.2.2. Fabrication of P(3-M-4-PAP)

P(3-M-4-PAP) was prepared by oxidative polycondensation reaction of 3-M-4-PAP in the presence of NaOCl oxidant in an aqueous alkaline medium (Scheme 1). 1 mmol (0.212 g) of 3-M-4-PAP was added in 0.2 M 10 mL KOH solution and it was dissolved under nitrogen atmosphere by refluxing. Then, NaOCl (3 mmol) was added in the monomer solution for 15 min after the planned polymerization temperature was reached. The yellow colored monomer solution was turned into dark brown as soon as NaOCl was added. After the planned polymerization time was over, the polymer in the obtained solution was precipitated with 1 M HCl. Then, the attained polymer was filtered, washed with hot methanol and water and dried at 80 °C.



Scheme 1. Preparation of 3-M-4-PAP, P(3-M-4-PAP) and Pd NPs@P(3-M-4-PAP) catalyst.

2.2.3. Generation of Pd NPs@P(3-M-4-PAP) catalyst

The immobilization of Pd NPs on P(3-M-4-PAP) was carried out without use of any reducing agent. Briefly, P(3-M-4-PAP) (0.3g) and PdCl₂ (0.1g) were introduced into 25 mL ethanol and refluxed at 70 °C for 24 h. Finally, the nanocatalyst was filtered, washed with ethanol and dried at 80 °C (Scheme 1).

2.2.4. Typical procedure for reduction of nitroarenes

0.1 mL of 0.05 M aqueous NaBH₄ solution which was freshly prepared was added on 1 mL of 1.0×10^{-4} M aqueous nitroarene solution in a tube. After the prepared solution was stirred for 1 min, 2 mg of the fabricated nanocatalyst was added in the produced solution. The final yellow mixture was stirred until its color became colorless and this process was also followed by UV–Vis analysis. Then, the nanocatalyst was filtered, rinsed with water (3×50 mL) and dried.

2.3. Characterization

Shimadzu Prominence Gel Permeation Chromatography attached Nucleogel GPC 103-5 VA300/7.7 column for GPC analysis was used to determine number average molecular weight (M_n), weight average molecular weight (M_w) and polydispersity index (PDI) values of the polymer (eluent: DMF, analysis temperature: 40 °C, flow rate: 0.5 mL/min, detector: refractive index detector (RID)). Shimadzu UV-1700 PharmaSpec UV–Visible Spectrophotometer was used to obtain UV–Vis spectra of the generated materials and nitroarenes. FTIR spectra of the fabricated products were attained by PerkinElmer FTIR Spectrometer (wavenumber range: 4000–650 cm⁻¹). ¹H NMR spectra of the products were recorded by Bruker Avance 500 MHz NMR in DMSO at 25 °C. TGA curves were obtained via EXSTAR S11 7300 Thermal Analyzer. Crystalline structure of the designed nanocatalyst was displayed by Rigaku Smart Lab X-Ray Diffractometer. SEM images and EDS analysis of the samples were acquired by FEI Quanta 450 FEG FE-ESEM-EDS. TEM images of Pd NPs@P(3-M-4-PAP) catalyst were attained by TEM JEOL JEM-2100 (UHR).

3. Results and discussion

3.1. Determination of optimum polymerization conditions

The effects of NaOCl concentration, polymerization time and temperature on the polymer yield were investigated and the obtained data were given in Fig. S1 (Please refer to Supplementary data). It was determined that the polymer yield (92.6%) increased

up to 0.3 mol/L NaOCl concentration but after this concentration, the yield gradually decreased (Fig. S1a). The polymer yield also increased up to 80° polymerization temperature and it decreased with increase in temperature after 80° (Fig. S1b). Moreover, the polymer yield increased up to 4 h polymerization time and after this time, it was seen a decrease in the yield with increase in polymerization time (Fig. S1c). The decrease in the yield with increase in NaOCl concentration and polymerization temperature and time may originate from formed shorter polymer chains due to high concentration of NaOCl and breaking in polymer chains at high temperature and time, respectively. Thus, broken and shortened chains may remove during washing of polymer [24–26]. Based on control experimental studies, the highest polymerization yield was reached using 0.3 mol/L NaOCl concentration at, 80 °C for 4 h.

3.2. Molecular weight distribution of P(3-M-4-PAP)

M_n , M_w and PDI values of P(3-M-4-PAP) which was synthesized under the determined optimum conditions were found by GPC analysis. The results displayed that the polymer had monomodal molecular weight distribution. The values for M_n , M_w and PDI were measured as 55475, 42368 g/mol and 1.30, respectively.

3.3. Structures of 3-M-4-PAP, P(3-M-4-PAP) and Pd NPs@P(3-M-4-PAP) catalyst

3.3.1. XRD analysis

XRD analysis were carried out to determine the crystalline structure of Pd NPs@P(3-M-4-PAP) catalyst (Fig. 1). The observed very broad peak at about 19° (2 θ) in the diagram of Pd NPs@P(3-M-4-PAP) catalyst can originate from the amorphous nature of the support; P(3-M-4-PAP). Moreover, five diffraction peaks were recorded at 40.3° (2 θ), 46.7° (2 θ), 68.5° (2 θ), 82.3° (2 θ) and 86.6° (2 θ) which can be indexed to (111), (200), (220), (311) and (222) diffractions of Pd and they can be ascribed to the face centered cubic palladium [2,27–30]. Also, the obtained diffraction peaks affirm the presence of palladium [2].

3.3.2. UV–Vis spectra

UV–Vis spectra of 3-M-4-PAP, P(3-M-4-PAP) and Pd NPs@P(3-M-4-PAP) catalyst are given in Supplementary data as Fig. S2. It

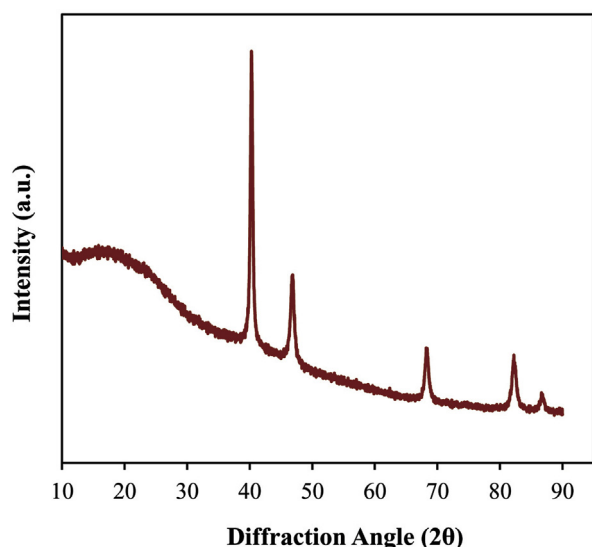


Fig. 1. XRD pattern of Pd NPs@P(3-M-4-PAP) catalyst.

was seen two absorption bands at 284 nm (π - π^* transitions of C=C_{benzene ring} and HC=N_{imine}) and 359 nm (n - π^* transition of OH functional group) in 3-M-4-PAP spectrum. These transitions could not be observed clearly in the polymer spectrum because of the increase in conjugation during the polymerization. When the polymer spectrum were compared to that of monomer, the under mentioned differences were seen in the polymer spectrum. i) Extension of the polymer spectrum to 700 nm, ii) becoming uncertain of the polymer bands by broadening reveal that the polymerization was actualized. Moreover, a broad band was determined at 331 nm in the Pd NPs@P(3-M-4-PAP) catalyst spectrum as distinct from that of the polymer. This band can originate from the surface plasmon resonance associated with the conversion of Pd^{II} to Pd⁰ [31].

3.3.3. FTIR spectra

FTIR spectra of the fabricated 3-M-4-PAP, P(3-M-4-PAP) and Pd NPs@P(3-M-4-PAP) catalyst are presented in Fig. 2. The peak belonging to vibration of HC=N- of 3-M-4-PAP was observed at 1626 cm⁻¹. This peak shifted to 1620 cm⁻¹ following to fabrication P(3-M-4-PAP), showing polymerization was successfully achieved and azomethine structure was protected during polymerization [23,24,32]. In case of Pd NPs@P(3-M-4-PAP), imine vibration shifted from 1620 cm⁻¹ to 1615 cm⁻¹ due to interaction of palladium with P(3-M-4-PAP). Moreover, the other important peaks indicating the structure of 3-M-4-PAP, P(3-M-4-PAP), and Pd NPs@P(3-M-4-PAP) catalyst can be arrayed as follows, respectively: OH vibrations at 3065, 3192, 3073 cm⁻¹, C–H stretching vibrations at 2904, 2924, 2923 cm⁻¹, C=C vibrations at 1591–1490, 1595–1470 and 1598–1436 cm⁻¹, aliphatic C–H bending vibrations at 1351, 1374,

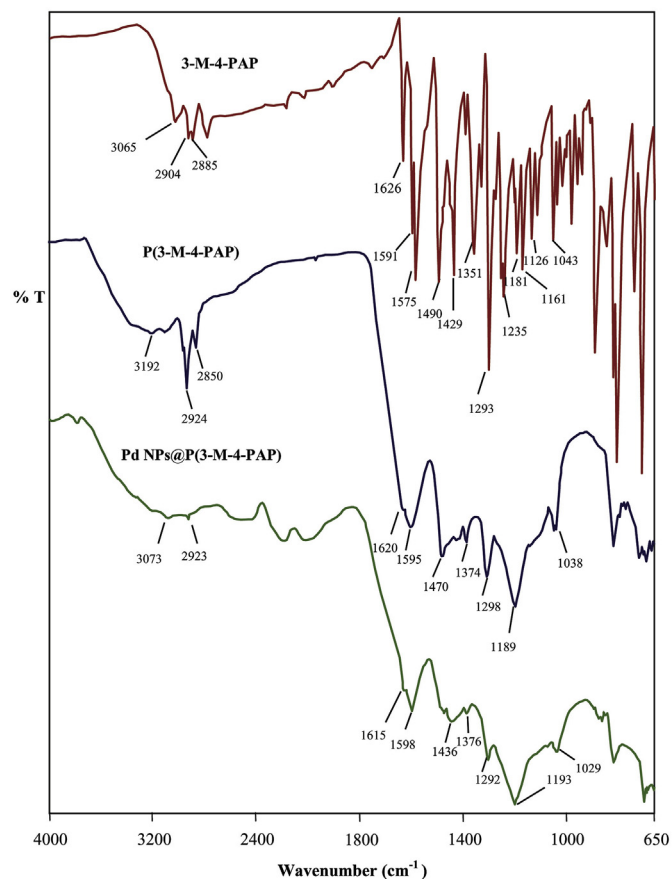


Fig. 2. FTIR spectra of 3-M-4-PAP, P(3-M-4-PAP) and Pd NPs@P(3-M-4-PAP) catalyst.

1376 cm^{-1} , C–O vibrations at 1235, 1189, and 1193 cm^{-1} , C–N vibrations at 1047, 1038 and 1043 cm^{-1} .

3.3.4. ^1H NMR spectra

^1H NMR spectra of 3-M-4-PAP and P(3-M-4-PAP) were recorded to verify their chemical structure. The signals of –OH, –CH=N- and –CH₃ functional groups of monomer were observed at 9.42 (s, 1H), 9.01 (s, 1H), and 2.28 ppm, respectively. These peaks were seen at 10.59 (s, 1H), 9.06 (s, 1H), and 2.26 ppm in the spectrum of polymer, respectively. The protons of aromatic structure of monomer were recorded at $\delta = 6.62$ (d, 1H); 6.67 (s, 1H); 7.05 (d, 1H); 7.49 (t, 1H); 8.26 (d, 1H); 8.56 (s, 1H) and 8.63 (d, 1H); ppm. These signals for polymer were also determined at $\delta = 8.78$ (d, 1H); 8.66 (s, 1H); 8.62 (t, 1H); 8.26 (d, 1H) and 7.56 (t, 1H) ppm. All these signals prove that the fabrication of 3-M-4-PAP and P(3-M-4-PAP) were successfully performed. Moreover, when the obtained signals of the monomer and polymer were compared to each other, it was detected that the polymerization of 3-M-4-PAP proceeded from C–C couplings formed from ortho positions of OH group.

3.3.5. Thermal degradation process

TGA curves of 3-M-4-PAP, P(3-M-4-PAP) and Pd NPs@P(3-M-4-PAP) to determine their thermal degradation behaviors are presented in Fig. 3. Also, the obtained results from TGA curves for the fabricated products are summarized in Table 1. As depicted in table, while the 50% weight losses of 3-M-4-PAP, P(3-M-4-PAP), and Pd NPs@P(3-M-4-PAP) occurred at 360, 618, and 961 $^{\circ}\text{C}$, 30% weight

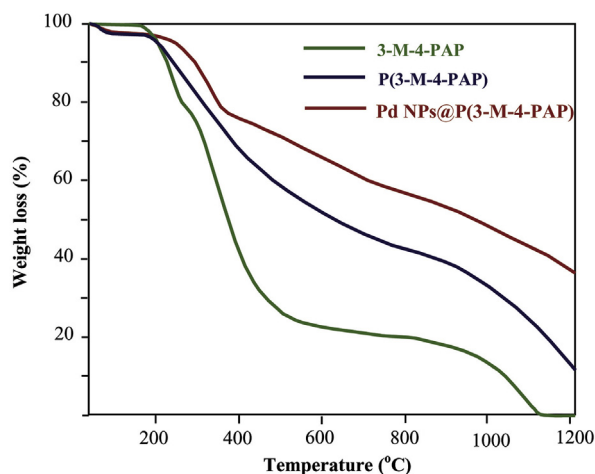


Fig. 3. TG curves of 3-M-4-PAP, P(3-M-4-PAP) and Pd NPs@P(3-M-4-PAP) catalyst.

Table 1

Thermal degradation data of 3-M-4-PAP, P(3-M-4-PAP) and Pd NPs@P(3-M-4-PAP) catalyst.

Compound	T_{on}^{a} ($^{\circ}\text{C}$)	Temperature ranges of weight loss stages ($^{\circ}\text{C}$)	Weight losses at each stage (%)	$T_{30\%}^{\text{b}}$ ($^{\circ}\text{C}$)	$T_{50\%}^{\text{c}}$ ($^{\circ}\text{C}$)	Residue at 1200 $^{\circ}\text{C}$ (%)
3-M-4-PAP	142	142–243	19.4	301	360	0
		243–600	57.9			
		600–1200	22.7			
P(3-M-4-PAP)	153	30–153	2.5	370	618	11.6
		153–600	46.1			
		600–1200	39.8			
Pd NPs@P(3-M-4-PAP)	155	30–155	2.0	513	961	37.8
		155–377	21.8			
		377–732	17.0			
		732–1200	21.4			

^a T_{on} represents the onset degradation temperature.

^b $T_{30\%}$ represents the temperature at which 30% weight losses occurred.

^c $T_{50\%}$ represents the temperature at which 50% weight losses occurred.

losses also were measured at 301, 370, and 513 $^{\circ}\text{C}$, respectively. These data show that while the polymer was more thermally stable compared to the monomer due to increasing conjugation in polymer backbone, the fabricated nanocatalyst was the most thermally stable product because of Pd⁰ content. Moreover, the carbon residues of 3-M-4-PAP, P(3-M-4-PAP) and Pd NPs@P(3-M-4-PAP) at 1200 $^{\circ}\text{C}$ were found as 0%, 11.6%, and 37.8%, respectively. The increase in carbon residue amount of the designed nanocatalyst originates the presence of Pd NPs.

3.3.6. FE-SEM and EDS analysis

FE-SEM analysis of 3-M-4-PAP, P(3-M-4-PAP) and Pd NPs@P(3-M-4-PAP) catalyst were performed to determine their surface morphologies and the sizes of the fabricated Pd NPs (Fig. 4). When FE-SEM image of 3-M-4-PAP in Fig. 6. a was examined, it was seen that the monomer had a flat, clean and smooth surface. Following the condensation reaction, the polymer which was prepared as support material also had a rougher and fissured surface with small particles compared to that of monomer (Fig. 4.b). Upon loading Pd NPs on the support material, the surface of the fabricated nanocatalyst was homogeneously covered with Pd NPs had smooth spherical shape (Fig. 4.c). Moreover, the size of the measured Pd NPs was also below 50 nm.

Moreover, EDS analysis of Pd NPs@P(3-M-4-PAP) was performed to find its elemental composition. EDS spectrum in Fig. 5 indicates the presence of C, O, N and Pd elements in composition of Pd NPs@P(3-M-4-PAP) catalyst. Additionally, while Pd content of Pd NPs@P(3-M-4-PAP) catalyst was determined as 29.28% by EDS analysis, this value was found as 29.95% by ICP analysis.

3.3.7. TEM analysis

TEM analysis of Pd NPs@P(3-M-4-PAP) was carried out for its further surface characterization and the recorded TEM images are given in Fig. 6. TEM images showed that Pd NPs were homogeneously dispersed on the surface of P(3-M-4-PAP). Moreover, it was found that average particle diameter of Pd NPs was determined as about 50 nm.

3.4. Catalytic efficiency of Pd NPs@P(3-M-4-PAP) catalyst in reduction of nitroarenes

Nitroarenes are known to be among of the most hazardous organic contaminants released to wastewaters from manufacturing plants and cause toxic, carcinogenic and mutagenic effects for all leaving creatures. Therefore, conversion of these detrimental chemicals to unarmful and useful products has become one of the most important issues in terms of both environment and industry.

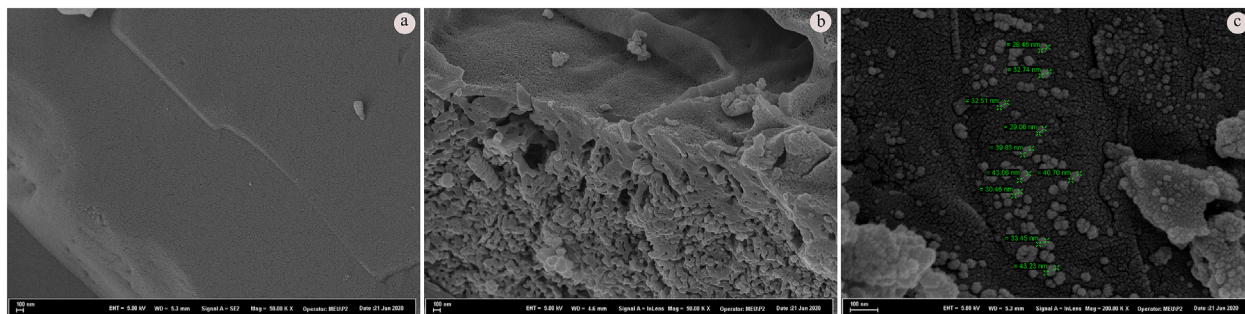


Fig. 4. FE-SEM micrographs of (a) 3-M-4-PAP, (b) P(3-M-4-PAP), and (c) Pd NPs@P(3-M-4-PAP) catalyst.

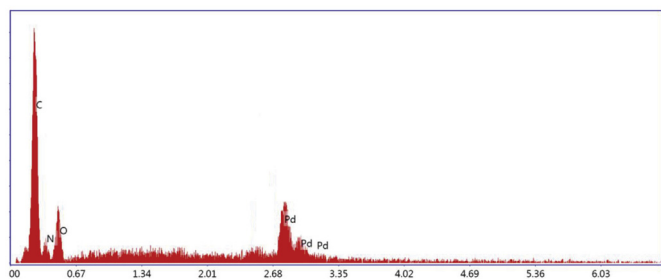


Fig. 5. EDS spectrum of Pd NPs@P(3-M-4-PAP) catalyst.

To be beneficial on behalf of the environment, catalytic ability of Pd NPs@P(3-M-4-PAP) catalyst was tested in reduction of several harmful nitroarenes to useful aniline derivatives using NaBH_4 in water media and all the reduction processes were followed by UV–Vis analysis. Firstly, the reduction of 4-NP to 4-AP was selected as the model reduction reaction. Then, the effects of catalyst amount and concentration of NaBH_4 on reduction time of 4-NP were investigated and the results are displayed in Table 2. As seen in table, when NaBH_4 concentration was increased in the reduction of 4-NP using same catalyst amounts, the reduction time gradually shortened due to increasing in hydrogen source in solution. When the reduction reactions were tested using 0.05, 0.0250, and 0.0125 M NaBH_4 concentrations in the presence of 2 mg

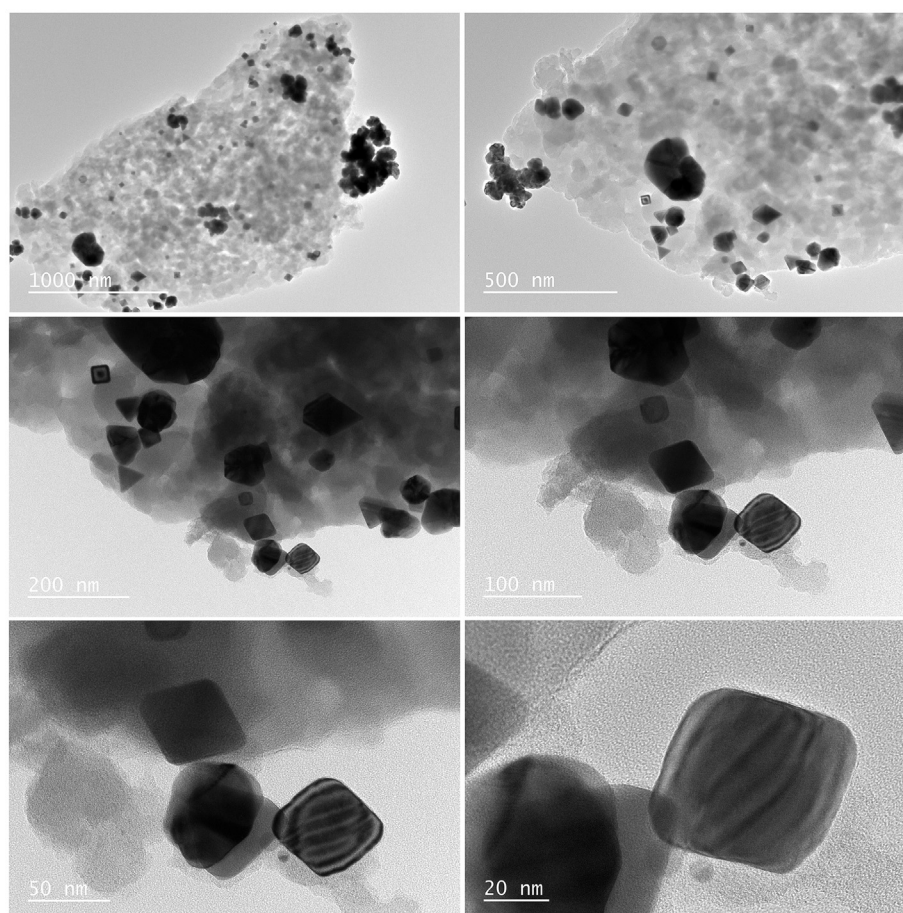


Fig. 6. TEM images of Pd NPs@P(3-M-4-PAP) catalyst.

Table 2
Reduction of 4-NP in the presence of Pd NPs@P(3-M-4-PAP) catalyst at different reaction conditions in water media.

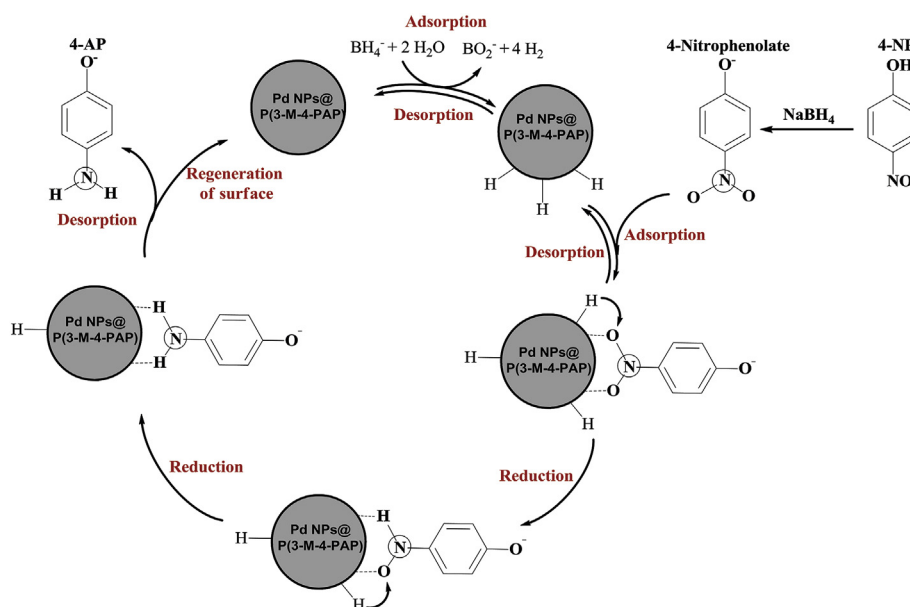
Entry	4-NP concentration (M)	NaBH ₄ concentration (M)	Catalyst amount (mg)	Reaction time (s)
1	1×10^{-4}	0.05	0.5	330
2	1×10^{-4}	0.05	1	100
3	1×10^{-4}	0.05	1.5	63
4	1×10^{-4}	0.05	2	40
5	1×10^{-4}	0.025	2	70
6	1×10^{-4}	0.0125	2	175
7	1×10^{-4}	0.1	0.5	55
8	1×10^{-4}	0.075	0.5	180
9	1×10^{-4}	0.075	1	83
10	1×10^{-4}	0.025	1	210

nanocatalyst, the reactions were completed within 40, 70 and 175 s. Since the shortest reduction time was obtained in the presence of 0.05 M NaBH₄, the next experiments were performed with this concentration. Upon increasing of amount of catalyst used, shortening in the reduction time was observed for same NaBH₄ concentrations. When it was used 0.5, 1.0, 1.5 and 2 mg catalyst amounts in the presence of 0.05 M NaBH₄ for reduction of 4-NP, the reductions were completed within 330, 100, 63, and 40 s, respectively. Consequently, since the shortest reduction time for 4-NP was attained using 2 mg Pd NPs@P(3-M-4-PAP) and 0.05 M NaBH₄, reduction reactions for all nitroarenes were performed under these conditions. Moreover, Scheme 2 displays probable mechanism for reduction of 4-NP to 4-AP using Pd NPs@P(3-M-4-PAP) catalyst. According to the feasible mechanism of 4-NP reduction, following the adsorption of 4-NP and BH₄⁻ ions on surface of Pd NPs@P(3-M-4-PAP) by π - π stacking interaction, BH₄⁻ ions containing the active hydrogen species are transferred to fabricate BO₂⁻ and H₂ gas. This operation may be catalyzed by palladium nanoparticles, to generate metal hydride complexes which were used as hydrogen mediators. In the nitroarenes reduction, to transfer electron from BO₂⁻ (donor) and 4-NP (acceptor), while Pd NPs can be used as oxidant, BH₄⁻ can be utilized as reductant, respectively. Finally, produced 4-AP is desorbed from Pd NPs@P(3-M-4-PAP) surface and then the catalytic reduction starts again.

The catalytic efficiency of Pd NPs@P(3-M-4-PAP) was evaluated in the reduction of eight different nitroarenes using NaBH₄ as

hydrogen source in water media under the determined optimum reaction conditions. While the obtained data are summarized in Table 3, UV-Vis spectra showing the reduction process of the nitroarenes are also displayed in Fig. 7. Before reduction process of 4-NP, strong absorption band was seen at 317 nm in its UV spectrum. When NaBH₄ was added in the solution, this band shifted to 400 nm, due to formation of 4-nitrophenolate ion (4-NPT) [33]. Upon adding the fabricated nanocatalyst in the resulting solution, while the absorption bands of 4-NPT disappeared by gradually decreasing within 40 s, simultaneously with this process, a new band was gradually observed at 300 nm which belong to 4-AP [34]. 3-nitrophenol (3-NP) displayed two typical absorption bands at 275 and 338 nm. Following the NaBH₄ addition in the solution of 3-NP, the band at 275 nm shifted to 295 nm and a new band appeared at 393 nm due to the production of 3-nitrophenolate (3-NPT). With the addition of the nanocatalyst in the solution, the peak at 393 nm disappeared and the peak at 295 nm shifted to 288 nm with in 35 s, verifying of the formation of 3-aminophenol (3-AP) [35]. It was also seen that the yellow color of the 4-NP and 3-NP solutions turned to straw yellow after NaBH₄ was added and this affirms formation of NPT. Moreover, after the catalytic reduction processes completely finished, the color of the resulting mixtures became colorless due to production of 4-AP and 3-AP.

In the reduction process of 2-NA, 4-nitroaniline (4-NA) and 4-nitro-*o*-phenylenediamine (4-NPD), firstly, two sharp absorption peaks were seen in their UV spectra at 283 and 410 nm; 227 and



Scheme 2. Proposed mechanism for the reduction of 4-NP using Pd NPs@P(3-M-4-PAP) catalyst.

Table 3
Catalytic reduction reactions of several nitroarenes to their aniline derivatives using NaBH₄ in the presence of Pd NPs@P(3-M-4-PAP) catalyst in water.

Entry	Nitro compound	Product	Reaction time (s)	Yield (%)
1			40	98
2			35	93
3			25	97
4			35	96
5			22	95
6			65	93
7			70	96
8			60	92
9 ^a			50	75

^a Reaction conditions: nitroarene = 1.0×10^{-4} M, NaBH₄ = 0.05 M, Pd NPs@P(3-M-4-PAP) = 2 mg, 1.0×10^{-4} M, NaBH₄ = 0.05 M, PdCl₂.

379 nm; 266 and 404 nm, respectively. While the bands at 410 nm, 379 nm and 404 nm vanished by gradually decreasing with adding Pd NPs@P(3-M-4-PAP) catalyst, the bands at 283 nm, 379 nm and 266 nm in spectra of 2-NA, 4-NA and, 4-NPDA, respectively, were also shifted simultaneously to 290 nm, 240 nm and 304 nm which belong to *o*-phenylenediamine (*o*-PDA), *p*-phenylenediamine (*p*-PDA) and benzene-1,2,4-triamine (BTA), respectively. The reduction reactions were completed within 25s, 35s and 22s for 2-NA, 4-NA and, 4-NPDA, respectively. Additionally, 4-nitrobenzoic acid (4-

NBA) was also reduced to 4-aminobenzoic acid (4-ABA) in 65s. The strong absorption peak of 4-NBA at 274 nm shifted to 263 nm after the reduction reaction was completed. 3-nitrobenzaldehyde (3-NB) and 4-nitrobenzaldehyde (4-NB) gave absorption peak at 233 nm and 267 nm in their UV spectra, respectively. After the catalytic reductions were completed, new peaks were seen at 282 nm and 286 nm. Also, the peaks at 233 and 267 nm shifted to 235 and 237 nm for 3-NB and 4-NB, respectively. These observations verified the reductions of 3-NB and 4-NB to 3-amino benzyl alcohol (3-ABA) and 4-amino benzyl alcohol (4-ABA), respectively. The catalytic reduction times were recorded as 45 s and 70 s for 3-NB and 4-NB, respectively. The reason of more slowly reduction of these compounds compared to other nitroarenes is the concomitant hydrogenation of both nitro group to amine and aldehyde group (CHO) to alcohol (OH) [36]. Moreover, to show catalytic superiority of prepared catalyst, control experiment performed by using PdCl₂ under the determined optimum reaction parameters on the model reduction reaction. After the reduction test in the presence of PdCl₂, reaction yield was determined as 75% within 50s. This result showed that Pd NPs@P(3-M-4-PAP) had higher activity than PdCl₂ salt and Pd NPs@P(3-M-4-PAP) had critical important against reduction of toxic nitro compounds.

Additionally, kinetic of reduction of 4-NP, which was selected as the model nitroarene reduction reaction, was investigated (Fig. 8). Since NaBH₄ concentration was much higher than 4-NP concentration, the rate of the reduction reaction is not dependent on the NaBH₄ concentration [37]. Thus, the catalytic reduction reaction of 4-NP followed pseudo-first-order kinetic model and the rate constant (k , s⁻¹), which was found from the plot of $\ln(c/c_0)$ versus the reaction time, was calculated to be 0.03 s⁻¹ according to the formula in below.

$$\ln(c/c_0) = \ln(A/A_0) = -kt$$

where c and c_0 state to the concentrations of 4-NP initially and at time t , respectively.

3.4.1. Reusability test for Pd NPs@P(3-M-4-PAP) catalyst

To be easily and fast recoverable and reusable of the any catalyst is of great importance in terms of industrial cost and applicability. Thus, reusability test for Pd NPs@P(3-M-4-PAP) catalyst was performed in reduction of 4-NP under optimum reduction conditions. In the recovery process, the nanocatalyst was filtered from the reaction mixture. After, the nanocatalyst was washed with ethanol and water, it was dried in an oven at 80 °C and it was used for the next cycle. As a result of performed 7 consecutive cycles, reduction times for each cycle are presented in Table S1 (Supplementary data). Pd NPs@P(3-M-4-PAP) catalyst successfully reduced 4-NP with 89% yield without great loss of its catalytic activity even after 7 consecutive recycle process. Additionally, ICP analysis was performed after the reusability test and very low leach (<1%) from catalyst was determined, confirming strong interaction of palladium with P(3-M-4-PAP).

Additionally, FTIR spectrum and FE-SEM micrographs of Pd NPs@P(3-M-4-PAP) catalyst which were recorded after seven successive runs showed that the chemical structure, surface morphology, particle shape and size of the nanocatalyst were similar with that of fresh nanocatalyst. These results indicated that the nanocatalyst could preserve its chemical structure and surface morphology even after consecutive seven runs. Thus, it can be expressed that Pd NPs@P(3-M-4-PAP) catalyst is an ideal nanocatalyst for nitroarenes reduction in terms of both industrial cost and environment.

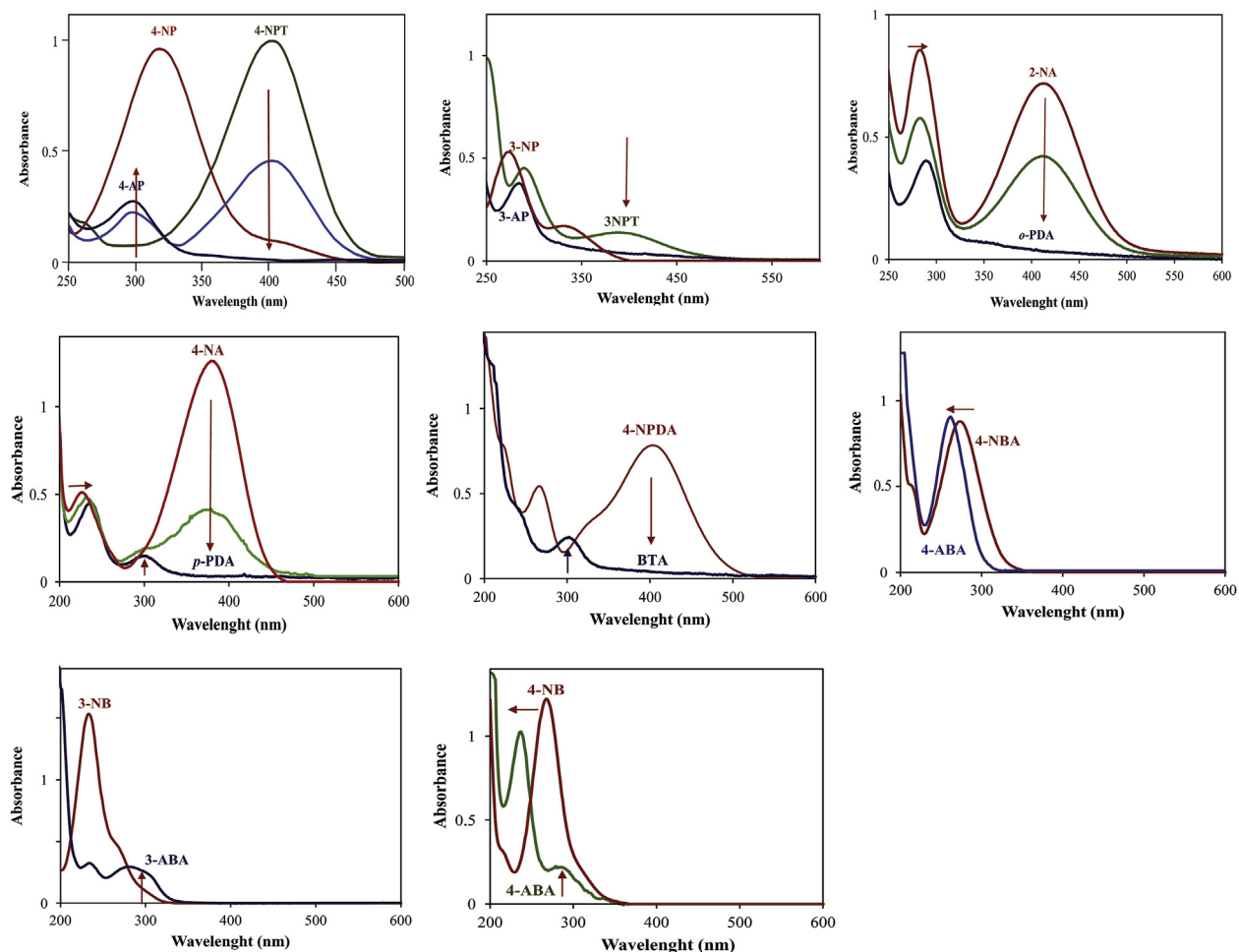


Fig. 7. UV–Vis spectra of the reduction of 4-NP, 3NP, 2-NA, 4-NA, 4-NPD, 4-NBA, 3-NB, and 4-NB to aniline derivatives using NaBH_4 in the presence of Pd NPs@P(3-M-4-PAP) catalyst in water. (Reaction conditions: nitroarene = 1.0×10^{-4} M, NaBH_4 = 0.05 M, Pd NPs@P(3-M-4-PAP) = 2 mg).

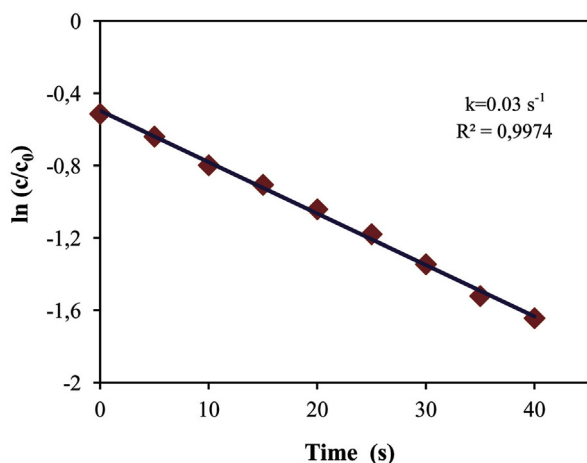


Fig. 8. Linear dependence graph between $\ln(c/c_0)$ and time for 4-NP reduction. (Reaction conditions: 4-NP = 1.0×10^{-4} M, NaBH_4 = 0.05 M, Pd NPs@P(3-M-4-PAP) = 2 mg).

4. Conclusions

In conclusion, this study presents the fabrication of highly active, easily and fast recoverable and recurrently reusable Pd NPs

immobilized on a novel polyazomethine with phenol group for reduction of harmful nitroarenes to useful aniline derivatives. The used analytical techniques affirmed the chemical structures of the synthesized 3-M-4-PAP, P(3-M-4-PAP) and Pd NPs@P(3-M-4-PAP) catalyst. Thermal analysis data showed that the P(3-M-4-PAP) support material and Pd NPs@P(3-M-4-PAP) catalyst had high thermal stability which is highly desired properties for industrial applications. The catalytic efficiency of generated nanocatalyst was tested in reduction of several harmful nitroarenes using NaBH_4 in water media at RT. The results indicated that Pd NPs@P(3-M-4-PAP) catalyst completely reduced all nitroarenes, which are very hazardous for all living creatures, at very short reaction times. Additionally, as a result of recoverability and reusability tests, it was determined that Pd NPs@P(3-M-4-PAP) catalyst was easily recoverable and it could be reusable seven consecutive runs by preserving its catalytic efficiency to a large extent. This efficient reusability and recoverability performance of Pd NPs@P(3-M-4-PAP) may play a significant role in industrial applications to reduce cost. The present study reveals that the fabricated Pd NPs@P(3-M-4-PAP) is an ideal catalyst for reduction of harmful nitroarenes to useful aniline derivatives.

Declaration of competing interest

The authors declare that they have no known competing financial interests or personal relationships that could have

appeared to influence the work reported in this paper.

CRedit authorship contribution statement

Nuray Yılmaz Baran: Methodology, Writing - original draft, Writing - review & editing, Data curation, Supervision.

Appendix A. Supplementary data

Supplementary data to this article can be found online at <https://doi.org/10.1016/j.molstruc.2020.128697>.

References

- [1] K.B. Narayanan, N. Sakthivel, Heterogeneous catalytic reduction of anthropogenic pollutant, 4-nitrophenol by silver-bionanocomposite using *Cylindrocodium floridanum*, *Bioresour. Technol.* 102 (2011) 10737–10740.
- [2] M. Atarod, M. Nasrollahzadeh, S. Mohammad Sajadi, Green synthesis of Pd/RGO/Fe₃O₄ nanocomposite using *Withania coagulans* leaf extract and its application as magnetically separable and reusable catalyst for the reduction of 4-nitrophenol, *J. Colloid Interface Sci.* 465 (2016) 249–258.
- [3] K. Naseem, R. Begum, Z.H. Farooqi, Catalytic reduction of 2-nitroaniline: a review, *Environ. Sci. Pollut. Control Ser.* 24 (2017) 6446–6460.
- [4] E. Farzad, H. Veisi, Fe₃O₄/SiO₂ nanoparticles coated with polydopamine as a novel magnetite reductant and stabilizer sorbent for palladium ions: synthetic application of Fe₃O₄/SiO₂/PDA/Pd for reduction of 4-nitrophenol and Suzuki reactions, *J. Ind. Eng. Chem.* 60 (2018) 114–124.
- [5] M. Nasrollahzadeh, Z. Issaabadi, R. Safari, Synthesis, characterization and application of Fe₃O₄@SiO₂ nanoparticles supported palladium(II) complex as a magnetically catalyst for the reduction of 2,4-dinitrophenylhydrazine, 4-nitrophenol and chromium(VI): a combined theoretical (DFT) and experimental study, *Separ. Purif. Technol.* 209 (2019) 136–144.
- [6] M.A. Oturan, J. Peirotan, P. Chartrin, A.J. Acher, Complete destruction of p-nitrophenol in aqueous medium by electro-fenton method, *Environ. Sci. Technol.* 34 (2000) 3474–3479.
- [7] S. Liu, Y.-J. Xu, Efficient electrostatic self-assembly of one-dimensional CdS–Au nanocomposites with enhanced photoactivity, not the surface plasmon resonance effect, *Nanoscale* 5 (2013) 9330–9339.
- [8] H. Börnick, P. Eppinger, T. Grischek, E. Worch, Simulation of biological degradation of aromatic amines in river bed sediments, *Water Res.* 35 (2001) 619–624.
- [9] N.E. Jiménez Jado, C. Fernández Sánchez, J.R. Ochoa Gómez, Electrochemical degradation of nitroaromatic wastes in sulfuric acid solutions: Part I, *J. Appl. Electrochem.* 34 (2004) 551–556.
- [10] P.C. Chen, W. Lo, K.H. Hu, Molecular structures of mononitroanilines and their thermal decomposition products, *Theor. Chim. Acta* 95 (1997) 99–112.
- [11] T. Baran, Biosynthesis of highly retrievable magnetic palladium nanoparticles stabilized on bio-composite for production of various biaryl compounds and catalytic reduction of 4-nitrophenol, *Catal. Lett.* 149 (2019) 1721–1729.
- [12] M. Nasrollahzadeh, Z. Issaabadi, S.M. Sajadi, Green synthesis of the Ag/Al₂O₃ nanoparticles using *Bryonia alba* leaf extract and their catalytic application for the degradation of organic pollutants, *J. Mater. Sci. Mater. Electron.* 30 (2019) 3847–3859.
- [13] M. Kumarraja, K. Pitchumani, Simple and efficient reduction of nitroarenes by hydrazine in faujasite zeolites, *Appl. Catal. Gen.* 265 (2004) 135–139.
- [14] X. Huang, H. Wu, S. Pu, W. Zhang, X. Liao, B. Shi, One-step room-temperature synthesis of Au@Pd core-shell nanoparticles with tunable structure using plant tannin as reductant and stabilizer, *Green Chem.* 13 (2011) 950–957.
- [15] M. Nasrollahzadeh, R. Akbari, Z. Issaabadi, S.M. Sajadi, Biosynthesis and characterization of Ag/MgO nanocomposite and its catalytic performance in the rapid treatment of environmental contaminants, *Ceram. Int.* 46 (2020) 2093–2101.
- [16] M. Nasrollahzadeh, E. Mehdipour, M. Maryami, Efficient catalytic reduction of nitroarenes and organic dyes in water by synthesized Ag/diatomite nanocomposite using *Alocasia macrorrhiza* leaf extract, *J. Mater. Sci. Mater. Electron.* 29 (2018) 17054–17066.
- [17] M. Bordbar, Z. Sharifi-Zarchi, B. Khodadadi, Green synthesis of copper oxide nanoparticles/clinoptilolite using *Rheum palmatum* L. root extract: high catalytic activity for reduction of 4-nitro phenol, rhodamine B, and methylene blue, *J. Sol. Gel Sci. Technol.* 81 (2017) 724–733.
- [18] P.T. Ahmad, B. Jaleh, M. Nasrollahzadeh, Z. Issaabadi, Efficient reduction of waste water pollution using GO/γ-MnO₂/Pd nanocomposite as a highly stable and recoverable catalyst, *Separ. Purif. Technol.* 225 (2019) 33–40.
- [19] M. Yıldırım, İ. Kaya, Synthesis and characterizations of poly(ether)/poly(phenol)s including azomethine coupled benzothiazole side chains: the effect of reaction conditions on the structure, optical, electrochemical, electrical and thermal properties, *Polym. Bull.* 71 (2014) 3067–3084.
- [20] D. Emdi Kaya, M. Saçak, Synthesis, characterization and antimicrobial properties of oligomer and monomer/oligomer–metal complexes of 2-[(Pyridine-3-yl-methylene)amino]phenol, *J. Inorg. Organomet. Polym.* 19 (2009) 286–297.
- [21] İ. Kaya, M. Yıldırım, A. Avcı, Synthesis and characterization of fluorescent polyphenol species derived from methyl substituted aminopyridine based Schiff bases: the effect of substituent position on optical, electrical, electrochemical, and fluorescence properties, *Synth. Met.* 160 (2010) 911–920.
- [22] İ. Kaya, E. Kartal, D. Şenol, Synthesis and characterization of polyphenol derived from Schiff bases containing methyl and carboxyl groups in the structure, *Des. Monomers Polym.* 18 (2015) 524–535.
- [23] C. Demetgül, A. Delikanlı, O.Y. Sarıbyık, M. Karakaplan, S. Serin, Schiff base polymers obtained by oxidative polycondensation and their Co(II), Mn(II) and Ru(III) complexes: synthesis, characterization and catalytic activity in epoxidation of styrene, *Des. Monomers Polym.* 15 (2012) 75–91.
- [24] N. Yılmaz Baran, M. Saçak, Synthesis, characterization and molecular weight monitoring of a novel Schiff base polymer containing phenol group: thermal stability, conductivity and antimicrobial properties, *J. Mol. Struct.* 1146 (2017) 104–112.
- [25] N. Yılmaz Baran, M. Saçak, Preparation of highly thermally stable and conductive Schiff base polymer: molecular weight monitoring and investigation of antimicrobial properties, *J. Mol. Struct.* 1163 (2018) 22–32.
- [26] N. Yılmaz Baran, M. Saçak, Molecular weight monitoring of poly(2-[[4-(dimethylamino)benzylidene]amino]phenol) depending on polymerization conditions: investigation of thermal stability, antimicrobial properties, and conductivity enhancement, *Adv. Polym. Technol.* 37 (2018) 3007–3016.
- [27] N. Gogoi, U. Bora, G. Borah, P.K. Gogoi, Nanosilica-anchored Pd(II)-Schiff base complex as efficient heterogeneous catalyst for activation of aryl halides in Suzuki–Miyaura cross-coupling reaction in water, *Appl. Organomet. Chem.* 31 (2017), e3686.
- [28] C. Sarmah, D. Sahu, P. Das, Anchoring palladium acetate onto imine-functionalized silica gel through coordinative attachment: an effective recyclable catalyst for the Suzuki–Miyaura reaction in aqueous-isopropanol, *Catal. Today* 198 (2012) 197–203.
- [29] T. Baran, Highly recoverable, reusable, cost-effective, and Schiff base functionalized pectin supported Pd(II) catalyst for microwave-accelerated Suzuki cross-coupling reactions, *Int. J. Biol. Macromol.* 127 (2019) 232–239.
- [30] T. Baran, M. Nasrollahzadeh, Cyanation of aryl halides and Suzuki–Miyaura coupling reaction using palladium nanoparticles anchored on developed biodegradable microbeads, *Int. J. Biol. Macromol.* 148 (2020) 565–573.
- [31] M. Nasrollahzadeh, S.M. Sajadi, E. Honarmand, M. Maham, Preparation of palladium nanoparticles using *Euphorbia thymifolia* L. leaf extract and evaluation of catalytic activity in the ligand-free Stille and Hiyama cross-coupling reactions in water, *New J. Chem.* 39 (2015) 4745–4752.
- [32] A. Özbülül, H. Mart, M. Tunçel, S. Serin, A new soluble Schiff base polymer with a double azomethine group synthesized by oxidative polycondensation, *Des. Monomers Polym.* 9 (2006) 169–179.
- [33] X. Gao, H. Zhao, Y. Liu, Z. Ren, C. Lin, J. Tao, Y. Zhai, Facile synthesis of PdNiP/Reduced graphene oxide nanocomposites for catalytic reduction of 4-nitrophenol, *Mater. Chem. Phys.* 222 (2019) 391–397.
- [34] J. Nimita Jebaranjitham, C. Mageshwari, R. Saravanan, N. Mu, Fabrication of amine functionalized graphene oxide – AgNPs nanocomposite with improved dispersibility for reduction of 4-nitrophenol, *Compos. B Eng.* 171 (2019) 302–309.
- [35] A. Zare Asadabadi, S.J. Hoseini, M. Bahrami, S.M. Nabavizadeh, Catalytic applications of β-cyclodextrin/palladium nanoparticle thin film obtained from oil/water interface in the reduction of toxic nitrophenol compounds and the degradation of azo dyes, *New J. Chem.* 43 (2019) 6513–6522.
- [36] Y. Su, X. Li, Y. Wang, H. Zhong, R. Wang, Gold nanoparticles supported by imidazolium-based porous organic polymers for nitroarene reduction, *Dalton Trans.* 45 (2016) 16896–16903.
- [37] Y. Zhang, S. Liu, W. Lu, L. Wang, J. Tian, X. Sun, In situ green synthesis of Au nanostructures on graphene oxide and their application for catalytic reduction of 4-nitrophenol, *Catal. Sci. Technol.* 1 (2011) 1142–1144.